ELSEVIER

Contents lists available at ScienceDirect

Earth and Planetary Science Letters

www.elsevier.com/locate/epsl



CO₂ and tectonic controls on Antarctic climate and ice-sheet evolution in the mid-Miocene



Anna Ruth W. Halberstadt ^{a,*}, Hannah Chorley ^b, Richard H. Levy ^{b,c}, Timothy Naish ^b, Robert M. DeConto ^a, Edward Gasson ^d, Douglas E. Kowalewski ^e

- ^a Climate System Research Center, University of Massachusetts, Amherst, MA 01003, United States of America
- ^b Antarctic Research Centre, Victoria University of Wellington, Wellington, 6012, New Zealand
- ^c GNS Science, Avalon, Lower Hutt 5040, New Zealand
- ^d School of Geographical Sciences, University of Bristol, Bristol, UK
- e Department of Earth, Environment, and Physics, Worcester State University, Worcester, MA 01602, United States of America

ARTICLE INFO

Article history: Received 10 October 2020 Received in revised form 19 February 2021 Accepted 23 March 2021 Available online 31 March 2021 Editor: Y. Asmerom

Dataset link: https://doi.org/10.7275/9wxa-yz16

Keywords:
Miocene
Antarctic ice sheet
ice sheet model
climate model
Transantarctic Mountain unlift

ABSTRACT

Antarctic ice sheet and climate evolution during the mid-Miocene has direct relevance for understanding ice sheet (in)stability and the long-term response to elevated atmospheric CO2 in the future. Geologic records reconstruct major fluctuations in the volume and extent of marine and terrestrial ice during the mid-Miocene, revealing a dynamic Antarctic ice-sheet response to past climatic variations. We use an ensemble of climate - ice sheet - vegetation model simulations spanning a range of CO2 concentrations, Transantarctic Mountain uplift scenarios, and glacial/interglacial climatic conditions to identify climate and ice-sheet conditions consistent with Antarctic mid-Miocene terrestrial and marine geological records. We explore climatic variability at both continental and regional scales, focusing specifically on Victoria Land and Wilkes Land Basin regions using a high-resolution nested climate model over these domains. We find that peak warmth during the Miocene Climate Optimum is characterized by a thick terrestrial ice sheet receded from the coastline under high CO2 concentrations. During the Middle Miocene Climate Transition, CO₂ episodically dropped below a threshold value for marine-based ice expansion. Comparison of model results with geologic data support ongoing Transantarctic Mountain uplift throughout the mid-Miocene. Modeled ice sheet dynamics over the Wilkes Land Basin were highly sensitive to CO2 concentrations. This work provides a continental-wide context for localized geologic paleoclimate and vegetation records, integrating multiple datasets to reconstruct snapshots of ice sheet and climatic conditions during a pivotal period in Earth's history.

© 2021 Elsevier B.V. All rights reserved.

1. Introduction

The mid-Miocene was significantly warmer than present and was characterized by a dynamic Antarctic Ice Sheet (AIS), with major fluctuations in the volume and extent of terrestrial and marine-based ice sheets (Gasson et al., 2016; Levy et al., 2016; Miller et al., 2020; Sangiorgi et al., 2018). Based on deep-ocean oxygen isotope sediment records, the Miocene Climatic Optimum (MCO; \sim 17–14.8 Ma) was identified as a period of unusual global warmth punctuating a long term cooling trend, during which the AIS was highly dynamic and fluctuated on orbital timescales (Flower and Kennett, 1994; Holbourn et al., 2013; Shevenell et al., 2008). The subse-

quent Middle Miocene Climate Transition (MMCT; 14.8–13.85 Ma) was characterized by interglacials that remained warm but glacials that increasingly intensified, culminating in one of the major cooling and ice expansion events during the Cenozoic evolution of the AIS. These prominent climatic variations have been attributed to atmospheric CO₂ drawdown, orbitally-driven temperature and precipitation variations, ocean circulation changes, and/or ocean gateway reconfiguration (e.g., Badger et al., 2013; Flower and Kennett, 1994; Holbourn et al., 2015; Levy et al., 2019; Shevenell et al., 2008). However, considerable uncertainty surrounds the climate and tectonic boundary conditions throughout the Miocene.

Geological data from a range of different proxies indicate that atmospheric CO₂ concentrations were higher than preindustrial levels during the MCO and decreased across the MMCT (Fig. S1). Various methods have been used to reconstruct past CO₂ through the mid-Miocene, together producing a wide range of estimates

^{*} Corresponding author.

E-mail address: ahalberstadt@umass.edu (A.R.W. Halberstadt).

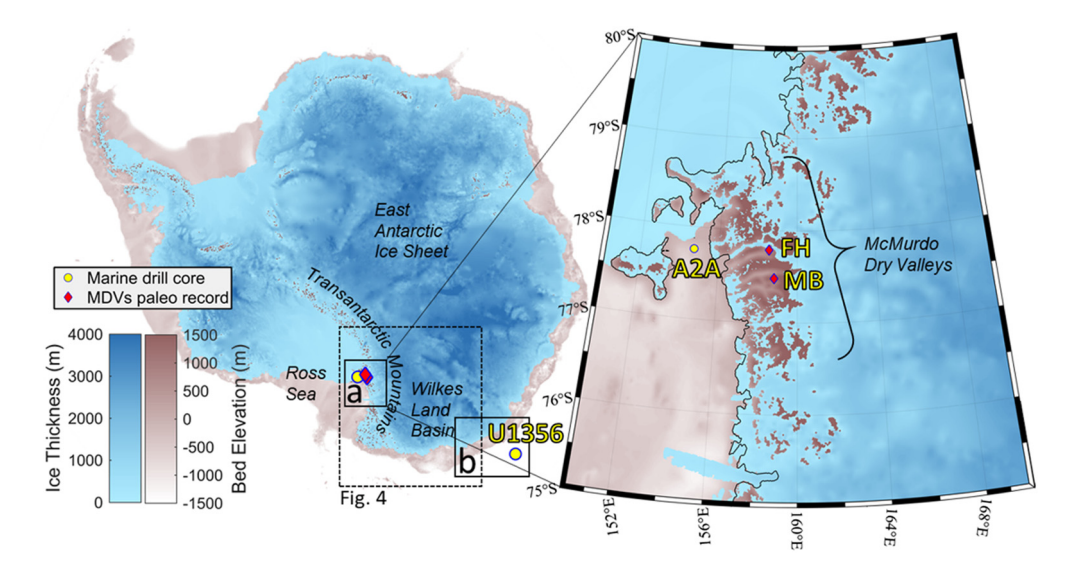


Fig. 1. Location of regions mentioned in text, along with paleo records used for model/data comparison (A2A: ANDRILL-2A, MB: Mt. Boreas, FH: Friis Hills), shown with modern ice thickness and bathymetry. For each model, we initiate 15-km-resolution nested RCMs across smaller domains: (a) Transantarctic Mountains region, to provide context for ANDRILL-2A and McMurdo Dry Valleys (MDVs) paleo records; and (b) offshore Wilkes Land Basin, to provide context for the U1356 drill core.

with values that range from 280 to over 800 ppm (Fig. S1), although work is ongoing to determine the most reliable proxy estimate for this time period.

The Transantarctic Mountains (TAM; Fig. 1), are a mountain chain over 5000 km long that divides the West Antarctic Rift System from the East Antarctic craton. Many of the key terrestrial geologic datasets spanning the Miocene are in or near the TAM (Fig. 1), and the reconstructed climate and ice-sheet implications of these records are highly sensitive to elevation. The northern and central TAM, at present-day peak elevations of >4000 m, have undergone a spatially and temporally complex uplift since the Cretaceous (e.g., Fitzgerald, 2002; Paxman et al., 2019a; Kerr et al., 2000). Glacial erosion and resulting isostatic uplift have further modified TAM elevations since ice-sheet inception at 34 Ma (Paxman et al., 2019b). The timing and interplay of thermal, tectonic, and erosional drivers of TAM uplift are relatively poorly constrained (Paxman et al., 2019a; Stern et al., 2005). Despite uncertainty over the style and timing of uplift, the TAM has played a significant role in the growth and stability of the East Antarctic Ice Sheet (EAIS), acting to buttress growth and limit ice flow through to the coast, but also as a focus of ice sheet nucleation (Gasson et al., 2016).

We explore the large uncertainties in CO₂ and TAM uplift by modeling the range of possible boundary conditions that could have produced the paleoenvironments reconstructed from geologic data. We investigate Antarctic climate and ice-sheet configuration under a range of past CO₂ concentrations, TAM uplift scenarios, and glacial/interglacial climates using coupled climate and ice-sheet models. Our work expands on previous model investigations of the mid-Miocene (e.g., Gasson et al., 2016; Langebroek et al., 2009) by including modeled CO₂ and topographic boundary conditions and implementing a detailed and systematic model/data comparison to evaluate our novel results.

2. Methods

Our model approach asynchronously couples an ice-sheet model (10 km resolution) with a global climate model (2° resolution) downscaled to a regional climate model over Antarctica (60 km resolution), and includes interactive vegetation. Nested climate models (Fig. 1a,b) are conducted at a 15 km resolution. To encompass all possible warm worlds throughout the Miocene, our model ensemble spans 280 ppm to 1140 ppm CO_2 . We use a

14 Ma Antarctic topographic reconstruction (Paxman et al., 2019b) that places the TAM at near-modern elevation with partial incision of TAM valleys. We hinged TAM elevations following a flexural cantilever model for TAM uplift (Stern and ten Brink, 1989), lowering the free end by 300 m, 500 m, and 800 m, and raising it by 300 m, to encompass all possible uplift histories. In addition to varying topography and CO₂, we simulate a 'glacial' or 'interglacial' climate that is independent of the prescribed atmospheric CO₂ concentration. 'Interglacial' climates are represented with an austral astronomical configuration favorable for Antarctic deglaciation and an additional Southern Ocean heat flux (Gasson et al., 2016); 'glacial' climates are represented with a cold austral astronomical configuration and no added heat flux.

We note that the CO_2 concentrations reported here are dependent on climate model physics, and should be placed into context within a long-standing challenge to model the reconstructed mid-Miocene warmth under relatively low CO_2 concentrations (e.g., Gasson et al., 2014; Langebroek et al., 2009). The climate models used in this study (GENESIS, downscaled with RegCM3) have a climate sensitivity of $2.9\,^{\circ}\text{C}$ warming per CO_2 doubling; for context, climate sensitivity in the most recent climate model intercomparison project ranges from $1.8\,^{\circ}\text{C}$ to $5.6\,^{\circ}\text{C}$ (CMIP6; Meehl et al., 2020). A climate model with higher climate sensitivity or increased polar amplification could satisfy the same geological constraints at lower modeled CO_2 ; therefore, CO_2 concentrations should be considered relative and not absolute.

3. Results

3.1. Antarctic ice sheet reconstructions

Our model ensemble spans a wide range of boundary conditions, providing a comprehensive picture of possible Miocene ice sheet configurations (Fig. 2). The largest ice sheet was produced by the lowest modeled CO₂ concentration (280 ppm) under a glacial climate; under these conditions, marine ice expanded out onto the continental shelf in a configuration with 135% volume of the modern ice sheet, accompanied by extensive perennial sea ice. Winter sea ice is prevalent around the ice sheet margin under 280 ppm CO₂ and an interglacial climate, but does not persist year-round. During 460 ppm glacials, small-scale marine ice advance coincides with widespread winter sea ice that persists only regionally throughout the summer. Interglacial climates with 460

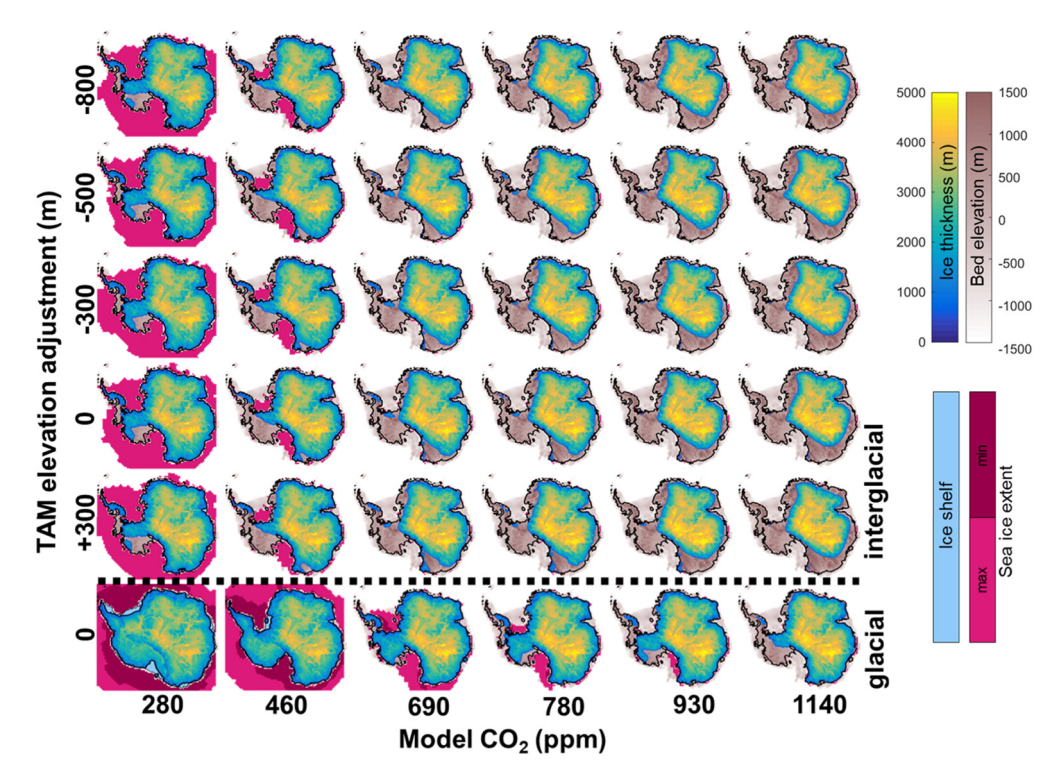


Fig. 2. Model ensemble results: equilibrated ice sheet configurations under varying astronomical orbits ('glacial' and 'interglacial'), topography, and CO₂ boundary conditions. Initial model topography (Paxman et al., 2019b) has an additional TAM elevation adjustment. Yearly sea ice variability is represented by plotting sea ice extent for the month where sea ice is at a minimum and the month where sea ice is at a maximum. On the upper rows, 'interglacial' climates are represented with an austral astronomical configuration favorable for Antarctic deglaciation and an additional Southern Ocean heat flux (Gasson et al., 2016); on the bottom row, 'glacial' climates are represented with a cold austral astronomical configuration and no added heat flux. Modeled ice sheets represent generic glacial or interglacial periods with constant boundary conditions.

ppm CO_2 (and glacial climates with higher CO_2 concentrations) produce regional winter sea ice only. The smallest ice sheet was produced by our warmest ensemble member, a 1140 ppm CO_2 interglacial. Despite this high atmospheric CO_2 concentration and warm interglacial ocean temperatures, the EAIS persists at $\sim 75\%$ of modern volume. Within our model ensemble, this ice sheet has the smallest footprint, with margins receded far from the coastline, but grows the thickest EAIS due to increased precipitation (central plateau elevations increase by about 800 m from 280 to 1140 ppm CO_2 under an interglacial climate).

Ice volume trends independent from the orbital glacial/interglacial cycle are influenced by an interplay of CO₂ concentration and TAM elevation. Unsurprisingly, elevated CO₂ concentrations lead to smaller ice volumes; lower TAM elevations are also associated with smaller ice volumes throughout the model ensemble, in part due to their buttressing effect on East Antarctic ice flowing toward the Ross Sea.

Some ice-free areas of the Antarctic continent were likely colonized by vegetation prior to the terminus of the MMCT; vegetation existed in the Ross Embayment during the mid-Miocene (Lewis et al., 2008). Our interactive vegetation model reproduced the unique biomes that develop under each set of boundary conditions within our model ensemble (Fig. 3). Tundra and boreal-like high latitude forests (taiga) are the most prevalent vegetation types, with interspersed desert and shrubland, and forest vegetation at the coast-line in the warmest interglacial worlds. With increasing CO₂ concentrations, the dominant biome transitions from tundra to taiga. Topographies with lower TAM elevations are warmer, initiating this biome shift at lower CO₂ concentrations.

3.2. Comparing model results with geologic data

Terrestrial and offshore paleo-environmental records can be used to constrain past CO₂ and TAM uplift boundary conditions

through comparison with our model results. We compile terrestrial and marine datasets from the mid-Miocene (Table S1). In the McMurdo Dry Valleys (MDVs), local temperature and paleoenvironment has been reconstructed from fossil assemblages including pollen, beetles, diatoms, and mosses (Lewis et al., 2008; Lewis and Ashworth, 2015). In addition to the terrestrial record, offshore marine drill cores provide a valuable record of regional ice dynamics and coastal temperatures; we complement the paleoenvironmental record from the MDVs with marine drill core data located adjacent to the TAM and offshore Wilkes Land Basin (WLB; Fig. 1). At each site, data-based paleoenvironmental reconstructions are compared to our ice sheet and climate model outputs to identify the range of past CO₂ and tectonic uplift scenarios that are consistent with the geologic record at that specific location (Fig. 4).

The Friis Hills and Mt. Boreas are single locations in the MDVs where fossil assemblages provide paleo-temperatures. Within our model ensemble, both locations are covered by an expanded EAIS under all glacial climates and under all interglacials with 280-460 ppm modeled CO₂ (Fig. 4a,b). An ice cap covers the MDVs under many remaining boundary conditions. Ice-free interglacials for both locations require a modeled CO₂ concentration of 690 ppm with low TAM elevations, and higher CO₂ at higher TAM elevations. However, we note that under some boundary conditions these locations are modeled as ice-covered but adjacent to an ice-free grid cell (Fig. 4a,b), which partly reflects the limitations of model resolution relative to point-sourced data locations. At the Friis Hills, reconstructed interglacial Mean Summer Temperatures (MSTs) of 6-7°C (Lewis and Ashworth, 2015) are reproduced by a range of boundary conditions in the model, with modeled $CO_2 \ge 690$ ppm (Fig. 4a). Mt Boreas similarly requires ≥690 ppm CO₂ and TAM elevations lower than modern (Fig. 4b) to reconstruct interglacial MSTs >5 °C (Lewis et al., 2008) but cooler conditions than the Friis Hills. Many model members grow ice over Mt. Boreas under boundary conditions that produce ice-free conditions at the

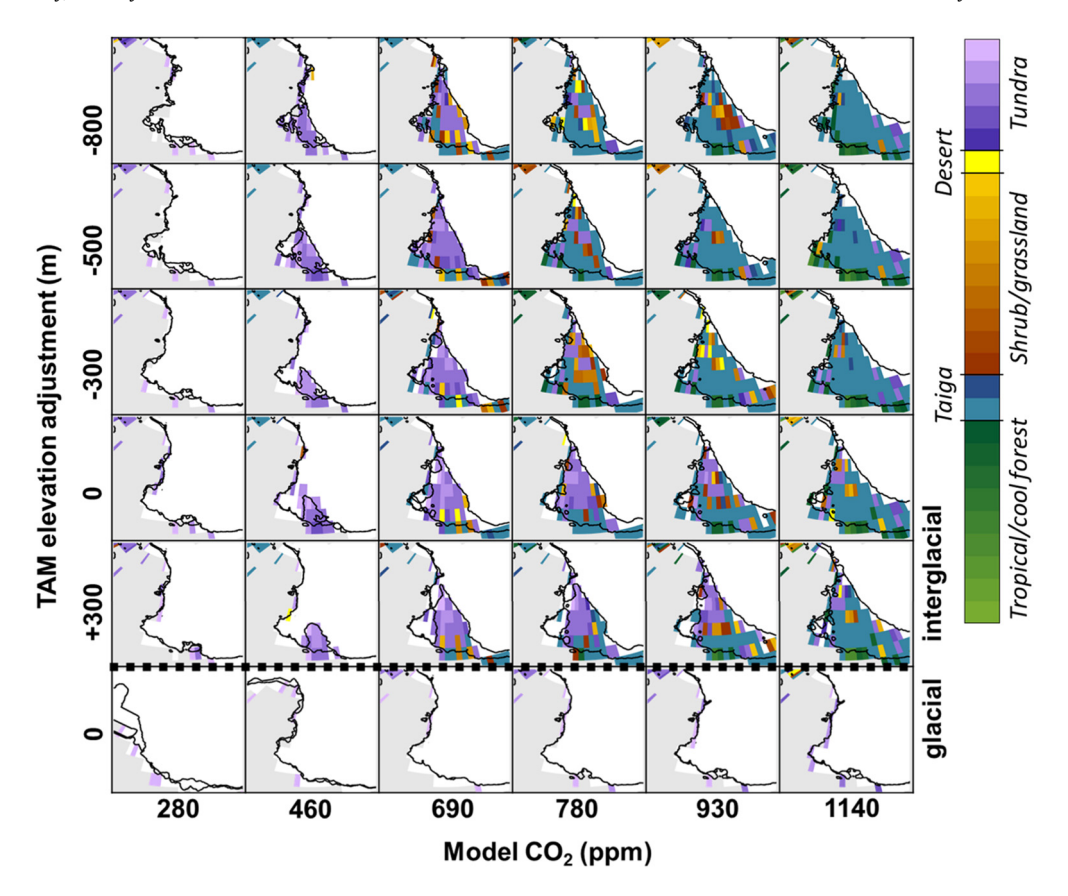


Fig. 3. Vegetation over the TAM region modeled using the BIOME4 interactive vegetation module (model resolution is $2^{\circ} \times 2^{\circ}$; black line shows 10 km-resolution ISM grounding line). The colorbar groups together biome outputs by vegetation type. Model runs under glacial conditions are shown in the bottom row; upper rows show runs under interglacial conditions.

nearby Friis Hills; because of the topographic and climatic complexity of the MDVs, it is likely that a higher model resolution would reveal that these same boundary conditions produce ice-free conditions (and relatively lower MSTs) at Mt. Boreas. Tundra paleo-environment has been inferred at both locations, ruling out model members with high CO_2 (≥ 930 ppm; Fig. 3).

We integrate these terrestrial data with information from marine drill core data. Only a few hundred kilometers from the MDVs, the ANDRILL-2A drill core preserves a sedimentary record in the Ross Sea spanning the early to middle Miocene (Levy et al., 2016; Passchier et al., 2011). This marine dataset reveals cyclical changes in coastal environments where ice occasionally advanced and retreated over the drill site and the surrounding TAM region, periodically allowing coastal tundra vegetation to flourish. We match each model member with one of the four environmental motifs described by Levy et al. (2016) to characterize the wider glaciological setting (Table S2; Fig. 5), and compare modeled glacial flowlines with paleo-ice-sheet flow reconstructions (Fig. S4).

Modelled terrestrial coastal temperatures near the ANDRILL-2A site generally remain below $0\,^{\circ}\text{C}$ during glacial periods (Fig. 4c). ANDRILL-2A palynological analysis suggests interglacial temperatures of <10\,^{\circ}\text{C}, with brief peak warmth episodes potentially reaching or exceeding $10\,^{\circ}\text{C}$ (Warny et al., 2009). These temperature ranges (7–10 $\,^{\circ}\text{C}$ and 10–11 $\,^{\circ}\text{C}$) match modeled interglacials with high CO₂ concentrations at all TAM elevations (Fig. 4c).

Geological drilling off the coast of Wilkes Land at site U1356 recovered a record of EAIS dynamics and paleoenvironment throughout the Miocene. Peak Miocene warmth is characterized by soil formation on extensive ice-free coastal lowlands, followed by episodic growth of marine-terminating ice (Sangiorgi et al., 2018). Our model ensemble reproduces a dynamic record of glaciation: the WLB is ice-covered during all modeled glacials, but ice-free

conditions prevail during interglacials under modeled CO_2 concentrations of 690 ppm and greater. Terrestrial fossil pollen assemblages from U1356 suggest MSTs $>10\,^{\circ}\text{C}$ (Sangiorgi et al., 2018), consistent with interglacial climates with CO_2 concentrations of 690 ppm and greater (Fig. 4d). In addition to MST, reconstructed mean annual temperatures from organic and inorganic chemistry are consistent with the same model members (Fig. S5), despite the uncertainties associated with both proxy and model approaches.

Sea ice was mostly absent throughout the MCO, appearing again across the MMCT (Levy et al., 2016; Sangiorgi et al., 2018). A lack of sea ice corresponds to modeled CO_2 concentrations \geq 780, while increased sea ice post-MCO suggests that CO_2 remained below 780 ppm at that time (Fig. 2). After the MCO, cooler marine and terrestrial temperatures and episodic ice-rafted debris suggest ice expansion punctuated by episodes of ice-sheet retreat leading to a reduced margin compared to the present day (Pierce et al., 2017; Sangiorgi et al., 2018), conditions which correspond to our interglacial worlds at 460 ppm CO_2 (Fig. 2).

4. Discussion

4.1. Implications for Miocene AIS evolution

Marine ice expansion and widespread perennial sea ice has been linked to systematic changes in ocean circulation and cryosphere development (DeConto et al., 2007; Flower and Kennett, 1994; Levy et al., 2019; Shevenell et al., 2008). We reconstruct expanded marine ice only under the coldest model boundary conditions (glacial climate with 280 ppm CO_2), and note that this expanded ice configuration is the only ensemble member characterized by significant ice shelves and perennial sea ice fringing

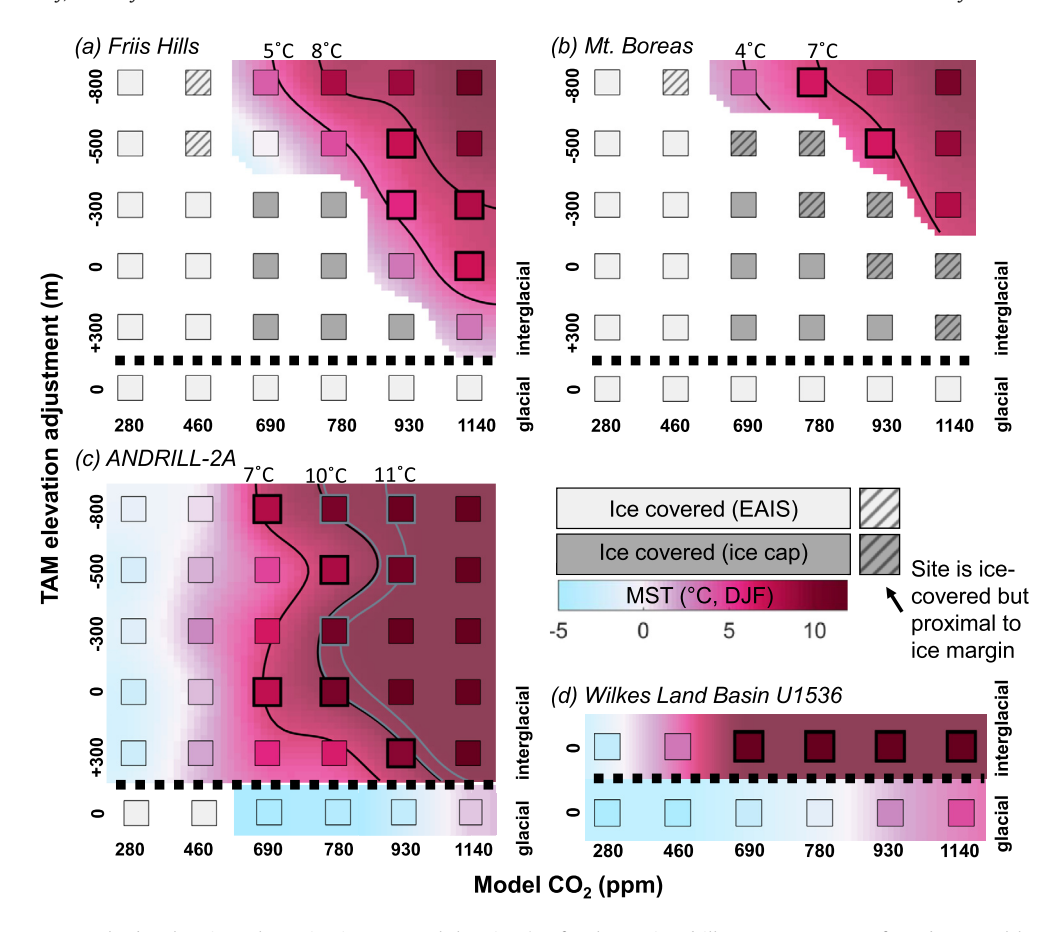


Fig. 4. Model temperatures at paleodata locations shown in Fig. 1. At each location (or, for the marine drill cores, an average of nearby coastal locations), we show mean summer temperature (MST) climate model output under each set of boundary conditions. Gray boxes indicate that the location is ice-covered, either by the East Antarctic Ice Sheet (EAIS; light gray) or an ice cap (dark gray). Thick black box outlines and contour lines indicate ensemble members and extrapolated boundary conditions, respectively, that satisfy the paleo-temperature constraints (Table S1). (a-b) MSTs at terrestrial locations (Friis Hills and Mt. Boreas); stippling indicates that the site is ice-covered but located <10 km from the ice margin. (c-d) MSTs for marine locations (ANDRILL-2A and U1536) are averaged from proximal coastal grid cells near the drill core site, representing the source of terrestrial pollen to the drill core. At ANDRILL-2A, black outlines denote temperatures 7–10°C, and gray outlines denote temperatures 10–11°C (interglacial temperatures and peak warmth, respectively; Warny et al., 2009). (d) At site U1356, offshore Wilkes Land Basin, we show only the original reconstructed topography because the TAM hinging region does not extend across this area (Fig. S3).

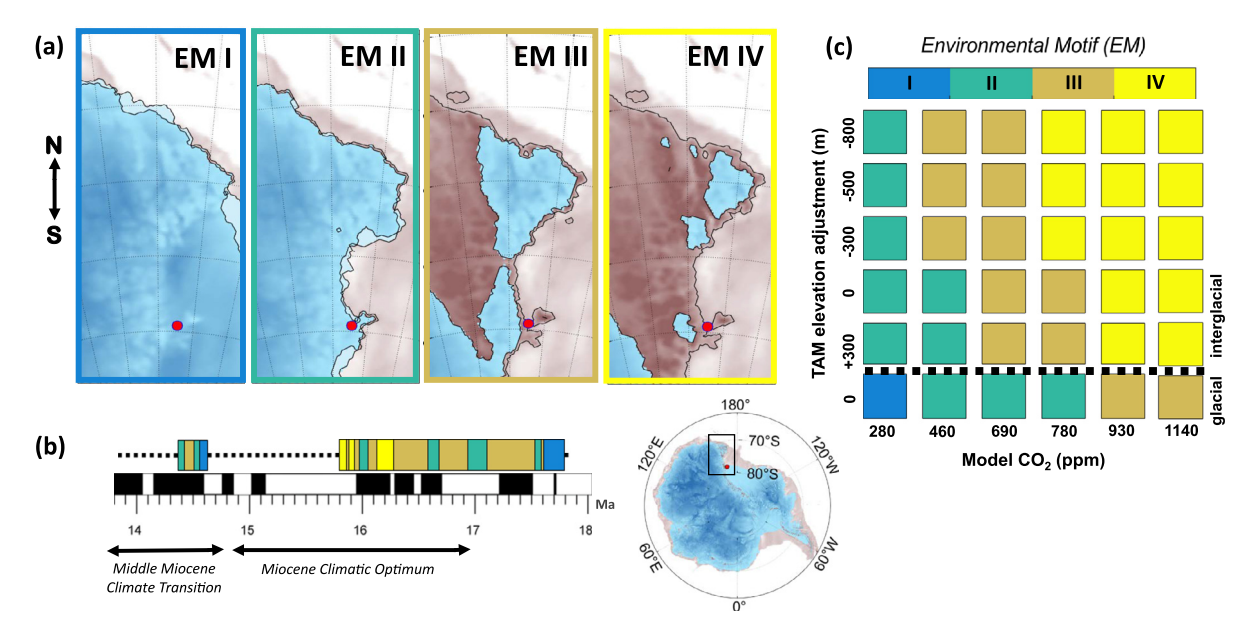


Fig. 5. (a) Model representation for each of the environmental motifs identified at the ANDRILL site (Levy et al., 2016), indicated by a circle. EM I is 'maximum ice' (grounded ice); EM II is 'cold polar' (coastal ice); EM III is 'cold temperate' (tidewater glaciation); and EM IV is 'minimum ice'. (b) Drill core recovery is represented with environmental motifs through time. (c) We assign an environmental motif for each ensemble model member (Table S2).

the continent (Fig. 2). This large marine-based ice sheet is consistent with geological observations of expanded Miocene marine ice sheets in the Ross Sea during and after the MMCT (Chow and Bart, 2003; De Santis et al., 1999; Passchier et al., 2011). However, 280 ppm is also the hypothesized threshold for the onset of largescale Northern Hemisphere glaciation (DeConto et al., 2008; Willeit et al., 2015). Given the lack of compelling evidence for Northern Hemisphere glaciation during the Miocene, and our reconstruction of small-scale marine advance around the fringes of our modeled 460 ppm glacial ice sheet, we suggest that the threshold for largescale marine-based ice growth in our models is below 460 ppm but higher than 280 ppm. Model CO₂ values depend on model climate sensitivity, however (Methods); this marine ice threshold can also be represented by a global mean land surface temperature increase of 2.4°C (from 13.7°C to 16.1°C between our 280 and 460 ppm glacial model members).

Although subject to model uncertainties, our process-based model results support inferences from previous stratigraphic studies of a marine ice threshold of approximately 400 ppm CO₂ (Badger et al., 2013; Levy et al., 2016, 2019; Naish et al., 2009), a key uncertainty in reconstructing past AIS dynamics.

We also note that our coldest ensemble member (glacial climate and 280 ppm CO_2 , representing an expanded marine ice sheet with 135% of modern volume) can still support vegetation refugia; isolated patches of tundra vegetation survive at the edge of the ice sheet (Fig. 3).

At the other climatic extreme, atmospheric warming under elevated CO2 concentrations drives recession of the terrestrial icesheet margins (Fig. 2) but warmer air temperatures also facilitate greater precipitation. Although strong orographic precipitation patterns over large ice sheets concentrate moisture at the margins with interior desert-like conditions, the greater moisture capacity of warmer air allows relatively more precipitation to reach the EAIS interior. EAIS growth during past warm periods has been linked to ocean transfer of heat and moisture from the low- and midlatitudes (DeConto et al., 2007; Schnitker, 1980; Shevenell et al., 2008), as well as albedo and cloud feedbacks (Goldner et al., 2013). Accordingly, our model produces thicker ice sheets in higher-CO₂ worlds (Fig. 2), highlighting the significance of relatively small precipitation changes integrated over the expansive polar plateau. These observations support the hypothesis that ice mass losses from future retreat of the EAIS margin onto land could be partially offset by thickening in the interior.

Our results indicate that increased precipitation in warmer worlds supports a thick EAIS plateau significantly receded inland from the coast (Fig. 2). These model reconstructions are consistent with proximal geologic data that suggest the ice sheet receded from the coastline during peak Miocene warmth (Levy et al., 2016; Passchier et al., 2011; Sangiorgi et al., 2018), although these records cannot constrain the inland extent of the EAIS. Our work reproduces large changes in ice volume at lower CO2 concentrations (280-460 ppm) but the EAIS remains insensitive to CO₂ at higher concentrations, which is broadly consistent with the relationship between CO2 and sea level documented by Foster and Rohling (2013) and Greenop et al. (2019). These studies suggest that full EAIS deglaciation occurs at CO2 concentrations of \sim 700–1000 ppm. The higher CO_2 threshold of EAIS stability in our results is concordant with previous ice-sheet modeling (Pollard and DeConto, 2005), and is also influenced by model climate sensitivity; at a higher equilibrium climate sensitivities, enhanced polar amplification may contribute to EAIS deglaciation at lower model CO₂ concentrations. Regardless of the model climate sensitivity, these model results are inconsistent with far-field sea level records indicating complete EAIS deglaciation during the MCO (Miller et al., 2020). This discrepancy reinforces the need for integrating proximal glacial records, process-based modeling, and far-field sea

level records to fully reconstruct ice-sheet stability during past warm periods.

Our model ensemble design explores the interplay between climate, tectonic forcings, and ice sheet evolution. Increasing $\rm CO_2$ above preindustrial levels exerts a greater influence on modeled ice-sheet volume than TAM elevation, although the TAM uplift scenario does impact the resulting ice sheet (Fig. 2). In cooler worlds with a full EAIS (e.g., 280 ppm), higher TAM elevations provide less vertical accommodation for a thick EAIS, but they serve to buttress EAIS growth and promote greater ice volume. In warm worlds where the TAM is mostly deglaciated, higher elevations remain cooler and can support larger ice caps, so ice volume is also greater. Therefore, we suggest that TAM uplift throughout the Miocene could have increased the capacity for continental ice growth under all $\rm CO_2$ concentrations.

Our reconstructions of large glacial/interglacial fluctuation of grounded ice across the WLB are consistent with geologic evidence of deglaciation of the WLB during warm periods (Cook et al., 2013; Pierce et al., 2017). With modeled CO₂ concentrations of 460 ppm or greater, the WLB is deglaciated during interglacials. Under 460 ppm boundary conditions, the shape of the WLB ice embayment is modulated by TAM elevation; at higher CO2 concentrations, the receded eastern margin remains consistent across all topographies and only the TAM ice cap on the western side is influenced by TAM elevation. During glacial periods under all CO₂ concentrations, ice regrows over the WLB (Fig. 2). We note that grounded marine ice in the Ross Sea (280 ppm glacials, and 460 ppm glacials to some extent) occurs only when the WLB is fully glaciated. Although the WLB remains exposed at relatively low-CO₂ interglacials, the Aurora Subglacial Basin appears to be less sensitive; we only reproduce significant deglaciation of this region under 1140 ppm CO₂.

4.2. Terrestrial records

Temperatures and ice configurations in the MDVs are highly sensitive to TAM uplift. Reconstructed temperatures at Friis Hills and Mt. Boreas are reproduced by our model under a range of boundary conditions (Fig. 4a,b), but these results must be carefully considered in light of model resolution issues. Despite the computational achievement of running an ensemble of nested climate models at 15 km resolution, this resolution is too coarse to fully capture the highly variable microclimates of the MDVs and small ice cap fluctuations across the complex and variable TAM topography. Nearby ice caps can insulate adjacent ice-free areas year-round; therefore, local topographic highs with small ice features may not be resolved in our model setup but could have a significant impact on local temperatures. The Friis Hills and Mt. Boreas were ice-covered during glacials and ice-free but located near the ice margin during interglacials (Lewis et al., 2008; Lewis and Ashworth, 2015), implying small scale glacial fluctuations potentially below the resolution of the nested climate model (15 km) or the ice-sheet model (10 km). Given the relatively coarse model resolution and complex topography of the MDVs, it is likely that a much wider range of boundary conditions can produce ice-free conditions at these sites (especially Mt. Boreas) but is not represented in our model approach. We acknowledge that MSTs of 5-6 °C at Mt. Boreas and 6-7 °C at Friis Hills may be achieved under a wider range of boundary conditions than shown in Fig. 4b, but our necessary model resolution masks these subtle variations in ice cover. Another source of uncertainty derives from the use of modern analogues to assign temperature ranges to fossil pollen assemblages; in addition to paleo-geographic differences, modern species may no longer mirror their fossil counterparts. We therefore recognize that the temperatures at Mt. Boreas and Friis Hills may not be significantly different from each other.

4.3. Marine records

Marine drill cores can record detailed regional information on past ice dynamics through time. Here, our ensemble of ice-sheet model reconstructions provides spatial context for the environmental facies identified at ANDRILL-2A (Fig. 5). Paleo-temperature reconstructions at this site match modeled coastal temperatures in our moderate to high-CO₂ interglacial simulations (Fig. 4c).

Grounded ice across the ANDRILL-2A drill site does not necessarily require the presence of the WAIS; both our modeled 280 and 460 ppm glacial worlds produce ice advance over the drill sites. However, an expanded marine-based ice sheet across the Ross Sea ('maximum ice' environmental motif, EM I) requires modeled CO2 to fall below 460 ppm; the 460 ppm glacial model is characterized by small-scale localized advance of marine ice sourced from the TAM (Fig. S4). The 'cold polar' environmental motif (EM II), interpreted as ice grounded at the coastline or slightly expanded into coastal marine environments and possibly forming an ice shelf, is produced only by the overriding of the EAIS through the TAM (Fig. S4). The 'cold temperate' motif (EM III), representing tidewater glaciation, is achieved in our model both with a full EAIS as well as a TAM ice cap (Fig. S4). EM III model members where the EAIS overrides the TAM have lower CO2 concentrations and higher TAM elevations, because lower CO₂ supports the growth of a large EAIS but high TAM elevations prevent ice from fully reaching the coast (EM II). At higher CO2 concentrations, we reconstruct EM III tidewater glaciation with a TAM ice cap expanded towards the coast.

Our model results provide valuable process-based context for ANDRILL-2A interpretations. Levy et al. (2016) divided their EM III motif into cooler (EM IIIa) and warmer (EM IIIb) environments. Here we also reconstruct diverging glacial environments within the EM III tidewater glaciation motif (TAM ice cap versus full EAIS); we add to their interpretation by suggesting that EM IIIa occurs at lower CO₂ concentrations with a full EAIS overriding the TAM, while EM IIIb is characterized by a local TAM ice cap. We also note that significant ice flow through the outlet glaciers north of Byrd Glacier occurs only when a full EAIS is connected to the TAM (Fig. S4); therefore, based on these results, sediments linked to Mulock or Skelton Glaciers could potentially interpreted as representative of EAIS overriding the TAM. This observation is borne out in the mineral provenance data at ANDRILL-2A; Mulock and Skelton glaciers contribute more sediment to the drill site during the cooler EM IIIa (Levy et al., 2016), when our model results would indicate a full EAIS. Generally, our modeled ice flowlines match mineral provenance reconstructions (Talarico et al., 2011) for interglacial conditions. Model flowlines (Fig. S4) indicate that Byrd Glacier was a significant EAIS outlet under all model boundary conditions used within our ensemble, and thus could have sourced sediment to the ANDRILL-2A site throughout the Miocene. This is consistent with the observation of coarse iceberg-rafted sediment delivered to the drill site even during warm environments (Levy et al., 2016).

Off the coast of Wilkes Land, pollen records captured in the U1356 marine drill core suggest that the WLB was characterized by warmer conditions than the TAM region, based on high pollen percentages of conifers and woody taxa diversity (Sangiorgi et al., 2018). Our model results uphold this interpretation; the high-resolution regional climate model over the TAM domain is consistently cooler than WLB, and is accentuated by higher TAM elevation adjustments. This temperature difference derives from topographical differences between the elevated TAM and lower, more coastal WLB/Adelie Coast, as well as a latitudinal difference between the two regions.

The U1356 site lacks evidence for marine ice or sea ice throughout the MCO (Sangiorgi et al., 2018). At higher CO_2 concentrations (780 ppm or greater), our modeled glacial ice sheets leave

a very thin ice-free zone at the coast, likely due to relatively warm ocean temperatures, which could have minimized marine-terminating glaciation and explain the lack of ice-rafted debris at the drill site during warmer glacial periods.

Sangiorgi et al. (2018) reconstruct episodic marine ice advances during the MMCT, accompanied by sea ice. Under glacial climates, our models produce ice expanded over the WLB to the coastline, with perennial sea ice under CO₂ concentrations < 690ppm. Our coldest model member, characterized by marine ice-sheet expansion elsewhere around the continent, does not produce grounded ice across the Wilkes Land continental shelf. Instead, our model shows large-scale marine-terminating glacial systems, capable of producing the ice-rafted debris pulses that reached site U1356 (Pierce et al., 2017; Sangiorgi et al., 2018) (Fig. 2; Fig. 6). This configuration is consistent with the conclusions of Pierce et al. (2017), who use provenance data from ice-rafted debris at site U1356 to conclude that the MMCT ice sheet expanded over the WLB but remained inland of its present location.

4.4. Characterizing the mid-Miocene

We constrain our ice-sheet and climate model results with available Miocene paleo-data from the TAM and WLB regions (Table S1) to highlight possible climatic and solid-Earth boundary conditions across major climatic events. Based on our model/data comparison approach, we investigate the evolution of atmospheric CO₂, TAM uplift, and ice-sheet dynamics during glacial and interglacial cycles throughout the Miocene. We provide potential model 'snapshots' of MCO and MMCT time periods that are consistent with the sparse geologic data (Fig. 6). Because the CO₂ values in our models are conditional on the model climate sensitivity, we consider our results to indicate approximate 'model CO₂' values rather than absolute values.

The Early Miocene ('pre-MCO'; Table S1) encompassed both warm interglacials as well as episodes of marine ice advance. The ANDRILL-2A record identifies short-lived intervals of the 'minimum ice' environment with proximal tundra vegetation; based on our model results, this would imply that CO₂ concentrations periodically exceeded 690 ppm (Fig. 5b,c). Moderately warm conditions (characterized by 'cold temperate' tidewater glaciation) imply a wide range of CO₂ concentrations (Fig. 5b,c) that are consistent with the Friis Hills record of an ice-free interglacial period (Fig. 4a). Marine ice occasionally advanced around the continent during early Miocene glacial periods (Levy et al., 2016; Passchier et al., 2011; Williams and Handwerger, 2005) (Fig. 5b), consistent with our modeled 460 ppm glacial world and therefore implying a CO₂ drop below approximately 460 ppm.

4.4.1. Miocene Climatic Optimum (MCO)

The MCO was an unusually warm time period (\sim 17–14.8 Ma). The ANDRILL-2A record reconstructs warm episodes across the MCO varying from 'cold temperate' tidewater glaciation to 'minimum ice' with coastal tundra vegetation associated with peak warmth (suggesting CO2 greater than 690 ppm and TAM elevations lower than modern; Fig. 5). 'Cold polar' conditions rarely occurred, suggesting that CO₂ remained well above 460 ppm (Fig. 5). ANDRILL-2A temperatures match modeled interglacials at 690 ppm CO₂ or greater; peak warmth reconstructions suggest CO₂ concentrations of 780 ppm or greater (Fig. 4c). MCO paleotemperatures at site U1356 also suggest relatively high CO2 concentrations (Fig. 4d). Based on the temperature constraints for the MCO (Fig. 4) and reconstructed environmental motifs (Fig. 5), our 690 and 780 ppm model simulations best capture MCO interglacial temperatures and MCO peak warmth, respectively, with TAM elevations at least below modern (Fig. 5c). At the Friis Hills, matching the reconstructed ice-free interglacial conditions for the late MCO under

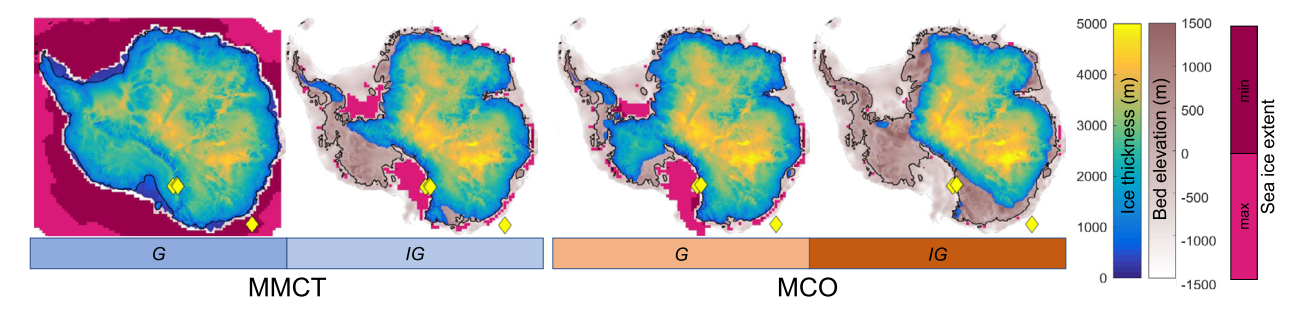


Fig. 6. Possible configurations for Middle Miocene Climatic Transition (MMCT) and Miocene Climate Optimum (MCO) worlds, where 'G' and 'IG' denote glacial and interglacial periods. The MCO interglacial snapshot represents peak warmth; the MMCT glacial snapshot reflects maximum ice extent. Locations of the relevant paleo-data records are shown for each time period (Fig. 1; Table S1).

these elevated CO_2 concentrations requires a TAM elevation adjustment of -500 m or greater (Fig. 4a).

We also constrain possible boundary conditions during the MCO using vegetation records, with the caveat that the coarse resolution of our vegetation model does not fully capture the regional topographic variability in the TAM. Vegetation reconstructions mainly consist of tundra (Lewis et al., 2008; Sangiorgi et al., 2018; Warny et al., 2009); Sangiorgi et al. (2018) also suggest that the WLB was characterized by a higher percentage and greater diversity of woody taxa than MDV records. Modeled 690 and 780 ppm interglacials generally satisfy these conditions, although the taiga biome begins to dominate over tundra at lower TAM elevations under 780 ppm CO₂ (Fig. 3).

To incorporate model/data comparisons of paleo-temperature, glacial environment, and vegetation, we suggest that MCO interglacials were characterized by elevated $\rm CO_2$ and TAM elevations at least 300 m lower than modern. We therefore infer that MCO peak warmth was characterized by receded ice caps and tundra along the TAM, widespread deglaciation of the WLB, and a substantial interior EAIS (Fig. 6). During glacials, the EAIS expanded to the coast.

4.4.2. Mid-Miocene climatic transition (MMCT)

During the MMCT, a large-scale climate transition from 14.8-13.8 Ma, glacial expansion appears to have successively intensified (e.g., Shevenell et al., 2008) (Fig. S1). The Friis Hills and Mt. Boreas sites record late MMCT interglacials with similar fossil assemblages as MCO interglacials (indicating relative warmth and characterized by tundra vegetation and ice-free but ice-proximal conditions), suggesting CO₂ > 460 ppm (Fig. 4a,b). 'Cold temperate' conditions characterized by tidewater glaciation are inferred at the ANDRILL-2A site during MMCT warm intervals, consistent with $CO_2 \ge 460$ ppm (Fig. 5). At site U1356, the MMCT was characterized by greater continental ice cover compared to the MCO, but interglacial episodes of warm water incursions drove smaller WLB ice configurations than modern with shrub tundra growing on the continent (Sangiorgi et al., 2018). These conditions are most compatible with our modeled 460 ppm CO₂ interglacial simulation, in which our ice-sheet model produces an interglacial WLB ice embayment configuration that matches the locations of inland bedrock erosion suggested by provenance of MMCT ice-rafted debris (Pierce et al., 2017). However, temperature constraints from the MDVs (Fig. 4a,b) are more consistent with our modeled simulations at 690 ppm CO₂ (or greater at lower TAM elevations).

Glacial periods across the MMCT increasingly intensified and expanded across the Ross Sea beginning around 14.6 Ma (Levy et al., 2016; Passchier et al., 2011). At the maximum ice extent, the EAIS overrode the MDVs (Lewis et al., 2008, 2007; Lewis and Ashworth, 2015), advanced across the Ross Sea (Chow and Bart, 2003; De Santis et al., 1999; Passchier et al., 2011) and expanded over the WLB (Sangiorgi et al., 2018). These reconstructions are

satisfied by our coldest modeled glacial simulation, with CO_2 concentrations below the threshold for marine ice advance (which we place slightly lower than 460 ppm). In our model, this marine ice threshold must be exceeded to grow ice over Prydz Bay, which is consistent with geologic data implying a prominent marine ice excursion during the MMCT (Florindo et al., 2003). We show that large-scale marine ice advance at the MMCT was accompanied by widespread perennial sea ice, which has been reconstructed by Levy et al. (2016) and Sangiorgi et al. (2018). Despite marine ice-sheet expansion elsewhere across the continent, grounded ice did not advance across the WLB continental shelf; instead, our model produces large-scale marine-terminating glacial systems capable of sourcing the ice-rafted debris at site U1356 (Pierce et al., 2017; Sangiorgi et al., 2018).

We suggest that CO_2 concentrations across the MMCT reached 460–690 ppm during warm interglacials but periodically dropped below 460 ppm to produce marine ice excursions and may have dropped to 280 ppm during maximum ice sheet expansion. An overall trend of declining CO_2 across the MMCT produced relatively cool interglacials characterized by a smaller-than-modern terrestrial ice sheet, punctuated by glacial periods when EAIS expanded to the coast, overriding the TAM and growing into the marine realm (Fig. 6). Although the growth of a large-scale marine ice sheet can be attained in our simulations by simply lowering CO_2 concentrations below 460 ppm, MMCT marine ice expansion was likely a response of the interplay between CO_2 drawdown, glacial feedbacks, and the significant changes in Southern Ocean circulation reconstructed at \sim 14 Ma.

4.4.3. TAM uplift

Estimates of TAM uplift throughout the Miocene vary. Rates of up to 100 m per million years are inferred from fission-track thermochronology (Fitzgerald, 1992), implying that mid-Miocene elevations could have been over 1 km lower than modern. Others have suggested that uplift since ~14 Ma was 300-800 m based on thermochronology and geomorphology (Miller et al., 2010), 300-400 m since the late Miocene based on diatom assemblages (e.g., Prentice and Krusic, 2005; Webb, 1974), less than 300 m since the Pliocene based on subaerial volcanic outcrops (Wilch et al., 1993), or 250 m since the Pliocene based on changes in dynamic topography (Austermann et al., 2015). Geomorphological studies suggest that modern elevations were attained by the end of the MMCT (Sugden et al., 1993) but that 400 m of subsidence occurred in the Miocene and was followed by 300 m of uplift in the Pliocene (Sugden et al., 1995). Clearly, TAM uplift history remains a topic of ongoing research. Although our model approach represents mountain uplift with a simple hinged cantilever (Stern and ten Brink, 1989), uplift was spatially and temporally complex and resulted from a complex and variable interplay of processes such as thermal uplift accompanying early rifting of the passive margin, thermal subsidence as the rift widened, and fluvial downcutting

driving isostatic uplift (e.g., Kerr et al., 2000; Stern and ten Brink, 1989). Different regions of the TAM have unique uplift histories; our model/data comparison is mainly based on paleoenvironmental records from the MDVs, so our results apply to primarily to the Dry Valleys block of the TAM which is thought to have been uplifted as one unit since the Early Tertiary (Fitzgerald, 2002).

Our model/data comparison of the MCO and MMCT time periods provides support for TAM uplift throughout the mid-Miocene. Across the MCO, modeled TAM elevations of at least 300 m below modern are consistent with geologic paleoenvironmental records. Modeled TAM elevations lowered by -300, -500 and -800 m can reproduce the reconstructed summer temperatures at the Friis Hills, the minimum-ice glacial environment reconstructed at the ANDRILL-2A site, and tundra vegetation along the TAM and WLB at lower (690 ppm) CO₂. Our model-based inference of at least 300 m of TAM uplift through the mid-Miocene is consistent with geological studies reconstructing post-mid-Miocene uplift (e.g., Austermann et al., 2015; Miller et al., 2010; Webb, 1974).

As glacial periods intensified across the MMCT, ice sheet overriding events likely drove valley erosion and corresponding isostatic rebound. We note that lower TAM elevations support more warm-based ice (Fig. S4), which could have driven additional erosion of these valleys as glaciers exploited the pre-existing fluvial landscape (e.g., Jamieson and Sugden, 2008). Thus, rising TAM elevations across the mid-Miocene could have contributed to a shift from wet-based to cold-based glaciation (Behrendt and Cooper, 1991) that is widely observed across the TAM at the same time (Lewis et al., 2007). Our model/data comparison suggests that isostatic response to sediment removal may have contributed to 800 m of uplift across the MMCT (our lowest modeled TAM elevation, which is still consistent with the paleoenvironmental record), causing the shift in basal thermal character inferred to have occurred between 14 and ~12 Ma.

4.4.4. Post-MMCT

Geologic records clearly show the extinction of vegetation from high elevations of the TAM at the end of the MMCT (Lewis et al., 2008; Lewis and Ashworth, 2015), which could have occurred due to a cooling climate driven by rising TAM elevations and decreasing CO₂ concentrations that we reconstruct from our model/data comparison. However, the presence of localized tundra vegetation in our model results suggest that despite extinction at high elevations, vegetation could have persisted in coastal lowlands beyond the MMCT. This is corroborated by geologic data from the DVDP-10 and -11 cores indicating that plants persisted at lower elevations in Taylor Valley until the Early Pliocene (Ohneiser et al., 2020), and palynological evidence for woody vegetation after the MMCT (Sangiorgi et al., 2018).

5. Summary and conclusions

We use asynchronously coupled ice-sheet and climate models under a range of different boundary conditions to reproduce mid-Miocene glacial and paleoenvironmental reconstructions across the TAM and WLB. Our model ensemble design explores the interplay between climate, mountain uplift, and ice sheet evolution.

Our results provide model-based support for geological reconstructions of large-scale marine ice expansion in the mid-Miocene at approximately 400 ppm CO₂, and was associated with the formation of perennial sea ice fringing the continent. Based on geologic evidence of marine-based ice sheets, CO₂ concentrations dropped below approximately 400 ppm several times during the early and mid-Miocene, and must have done so consistently across the MMCT. Even during these episodes of marine ice expansion, isolated patches of tundra vegetation survived at the edge of the ice sheet. With increasing CO₂ concentrations (above 280 ppm), we

model dynamic ice-sheet behavior over WLB, with a full cycle of advance and retreat between glacials and interglacials, consistent with geologic evidence for vulnerability of this region. We match model ensemble members with ANDRILL-2A environmental motifs, providing process-based spatial context to extrapolate drill core interpretations.

Model climate under a range of boundary conditions can be directly compared to mid-Miocene paleoenvironmental conditions to characterize glacial and interglacial periods across the MCO and MMCT and to extrapolate wider glacial conditions from reconstructed paleoenvironment at limited locations. We suggest that MCO peak warmth is most consistent with our modeled interglacial simulations at 690–780 ppm $\rm CO_2$, characterized by small TAM ice caps surrounded by tundra and widespread deglaciation of the WLB. During peak Miocene warmth, we model a thick EAIS receded from the coastline (\sim 85-90% modern volume), driven by greater moisture delivery in a warmer atmosphere.

During MMCT interglacials, ice cover over the WLB was greater than during MCO interglacials but smaller than present. The TAM was characterized by tidewater glaciation and tundra vegetation, with ice-free but ice-proximal conditions at the Friis Hills and Mt. Boreas sites. Reconstructed paleoenvironment and temperatures are most consistent with our modeled interglacial simulations at 460–690 ppm CO₂. Declining CO₂ across the MMCT exceeded the threshold for marine-based ice sheet growth during some glacial periods, driving the expansion of grounded ice into marine embayments around the continent. Grounded ice did not advance across the WLB continental shelf, instead forming large marine-terminating systems at the coastline.

We hypothesize that TAM uplift was ongoing throughout the mid-Miocene; modeled TAM elevations of at least 300 m below modern are consistent with geologic paleoenvironmental records across the MCO. Lower modeled TAM elevations (500–800 m below present) produce modeled climates that better satisfy the reconstructed glacial conditions and temperature around the TAM but are less consistent with our vegetation reconstructions. As the TAM uplifted, rising elevations could have supported the growth of greater ice volumes under all CO₂ concentrations. Progressive valley erosion during intensifying glacial advances across the MMCT likely contributed to isostatic uplift of the valleys and may have driven the shift from wet-based to cold-based glaciation across this transition.

CRediT authorship contribution statement

All authors designed the research; A.R.W.H. and H.C. performed research; all authors analyzed data; and A.R.W.H. wrote the paper with input from all authors.

Declaration of competing interest

The authors declare that they have no known competing financial interests or personal relationships that could have appeared to influence the work reported in this paper.

Data availability

Model output for all ensemble members is available through the UMass Library Data Repository at https://doi.org/10.7275/9wxa-yz16.

Acknowledgements

We thank Joe Prebble and Sophie Warny for helpful guidance on pollen data interpretation. A.R.W.H. was supported US National Science Foundation Award ICER 1664013. The Friis Hills field season was supported by NSF-1638954, and the US Antarctic Program and Antarctica New Zealand. Funding support for R.L., T.N., and H.C. was provided by the New Zealand Ministry of Business, Innovation and Employment through the Past Antarctic Science Programme (C05X1001) and Antarctic Science Platform (ANTA1801). Additional support for H.C. was provided through a Victoria University of Wellington PhD scholarship. E.G. is supported by a Royal Society Fellowship grant URF\R1\180317.

Appendix A. Supplementary material

Supplementary material related to this article can be found online at https://doi.org/10.1016/j.epsl.2021.116908.

References

- Austermann, J., Pollard, D., Mitrovica, J.X., Moucha, R., Forte, A.M., DeConto, R.M., Rowley, D.B., Raymo, M.E., 2015. The impact of dynamic topography change on Antarctic ice sheet stability during the mid-Pliocene warm period. Geology 43, 927–930. https://doi.org/10.1130/G36988.1.
- Badger, M.P.S., Lear, C.H., Pancost, R.D., Foster, G.L., Bailey, T.R., Leng, M.J., Abels, H.A., 2013. CO2 drawdown following the middle Miocene expansion of the Antarctic Ice Sheet. Paleoceanography 28, 42–53. https://doi.org/10.1002/palo.20015.
- Behrendt, J.C., Cooper, A., 1991. Evidence of rapid Cenozoic uplift of the shoulder escarpment of the Cenozoic West Antarctic rift system and a speculation on possible climate forcing. Geology 19, 315–319. https://doi.org/10.1130/0091-7613(1991)019<0315:FORCIJO>2.3.CO:2.
- Chow, J.M., Bart, P.J., 2003. West Antarctic Ice Sheet grounding events on the Ross Sea outer continental shelf during the middle Miocene. Palaeogeogr. Palaeoclimatol. Palaeoecol. 198, 169–186. https://doi.org/10.1016/S0031-0182(03)00400-0.
- Cook, C.P., Van De Flierdt, T., Williams, T., Hemming, S.R., Iwai, M., Kobayashi, M., Jimenez-espejo, F.J., Escutia, C., González, J.J., Khim, B., Mckay, R.M., Passchier, S., Bohaty, S.M., Riesselman, C.R., Tauxe, L., Sugisaki, S., Galindo, A.L., 2013. Dynamic behaviour of the East Antarctic ice sheet during Pliocene warmth. Nat. Geosci. 6, 765-769. https://doi.org/10.1038/ngeo1889.
- De Santis, L., Prato, S., Brancolini, G., Lovo, M., Torelli, L., 1999. The Eastern Ross Sea continental shelf during the Cenozoic: Implications for the West Antarctic ice sheet development. Glob. Planet. Change 23, 173–196. https://doi.org/10.1016/S0921-8181(99)00056-9.
- DeConto, R., Pollard, D., Harwood, D., 2007. Sea ice feedback and Cenozoic evolution of Antarctic climate and ice sheets. Paleoceanography 22, 1–18. https://doi.org/ 10.1029/2006PA001350.
- DeConto, R.M., Pollard, D., Wilson, P.a., Pälike, H., Lear, C.H., Pagani, M., 2008. Thresholds for Cenozoic bipolar glaciation. Nature 455, 652–656. https://doi.org/ 10.1038/nature07337
- Fitzgerald, P., 2002. Tectonics and landscape evolution of the Antarctic plate since the breakup of Gondwana, with an emphasis on the West Antarctic Rift system and the Transantarctic Mountains. R. Soc. N. Z. Bull. 35, 453–469.
- Fitzgerald, P.G., 1992. The Transantarctic Mountains of southern Victoria Land: the application of apatite fission track analysis to a rift shoulder uplift. Tectonics 11, 634–662.
- Florindo, F., Bohaty, S.M., Erwin, P.S., Richter, C., Roberts, A.P., Whalen, P.A., Whitehead, J.M., 2003. Magnetobiostratigraphic chronology and palaeoenvironmental history of Cenozoic sequences from ODP sites 1165 and 1166, Prydz Bay, Antarctica. Palaeogeogr. Palaeoclimatol. Palaeoecol. 198, 69–100. https://doi.org/10.1016/S0031-0182(03)00395-X.
- Flower, B.P., Kennett, J.P., 1994. The middle Miocene climatic transition: East Antarctic ice sheet development, deep ocean circulation and global carbon cycling. Palaeogeogr. Palaeoclimatol. Palaeoecol. 108, 537–555.
- Foster, G.L., Rohling, E.J., 2013. Relationship between sea level and climate forcing by CO2 on geological timescales. Proc. Natl. Acad. Sci. 110, 1209–1214. https:// doi.org/10.1073/pnas.1216073110.
- Gasson, E., DeConto, R.M., Pollard, D., Levy, R.H., 2016. Dynamic Antarctic ice sheet during the early to mid-Miocene. Proc. Natl. Acad. Sci. 201516130. https://doi. org/10.1073/pnas.1516130113.
- Gasson, E., Lunt, D.J., Deconto, R., Goldner, A., Heinemann, M., Huber, M., Legrande, A.N., Pollard, D., Sagoo, N., Siddall, M., Winguth, A., Valdes, P.J., 2014. Uncertainties in the modelled CO2 threshold for Antarctic glaciation. Clim. Past 10, 451–466. https://doi.org/10.5194/cp-10-451-2014.
- Goldner, A., Huber, M., Caballero, R., 2013. Does Antarctic glaciation cool the world? Clim. Past 9, 173–189. https://doi.org/10.5194/cp-9-173-2013.
- Greenop, R., Sosdian, S.M., Henehan, M.J., Wilson, P.A., Caroline, H., Foster, G.L., 2019. Orbital forcing, ice-volume and CO2 across the Oligocene-Miocene transition. Paleoceanogr. Paleoclimatol. 34, 316–328. https://doi.org/10.1029/ 2018PA003420.

- Holbourn, A., Kuhnt, W., Clemens, S., Prell, W., Andersen, N., 2013. Middle to late Miocene stepwise climate cooling: evidence from a high-resolution deep water isotope curve spanning 8 million years. Paleoceanography 28, 688–699. https:// doi.org/10.1002/2013PA002538.
- Holbourn, A., Kuhnt, W., Kochhann, K.G.D., Andersen, N., Sebastian Meier, K.J., 2015. Global perturbation of the carbon cycle at the onset of the Miocene Climatic Optimum. Geology 43, 123–126. https://doi.org/10.1130/G36317.1.
- Jamieson, S.S.R., Sugden, D.E., 2008. Landscape evolution of Antarctica. In: Cooper, A.K., Barrett, P.J., Stagg, H., Storey, B., Stump, E., Wise, W., and the 10th ISAES Editorial Team (Eds.), Antarctica: a Keystone in a Changing World. Proceedings of the 10th International Symposium on Antarctic Earth Sciences. The Nati, Washington, DC, pp. 39–54.
- Kerr, A., Sugden, D.E., Summerfield, M.A., 2000. Linking tectonics and landscape development in a passive margin setting: the Transantarctic Mountains. In: Geomorphology and Global Tectonics. John Wiley and Sons, pp. 303–319.
- Langebroek, P.M., Paul, A., Schulz, M., 2009. Antarctic ice-sheet response to atmospheric CO2 and insolation in the Middle Miocene. Clim. Past 5, 633–646. https://doi.org/10.5194/cp-5-633-2009.
- Levy, R., Harwood, D., Florindo, F., Sangiorgi, F., Tripati, R., Von Eynatten, H., Gasson, E., Kuhn, G., Tripati, A., DeConto, R., Fielding, C., Field, B., Golledge, N., Mckay, R., Naish, T., Olney, M., Pollard, D., Schouten, S., Talarico, F., Warny, S., Willmott, V., Acton, G., Panter, K., Paulsen, T., Taviani, M., 2016. Antarctic ice sheet sensitivity to atmospheric CO2 variations in the early to mid-Miocene. Proc. Natl. Acad. Sci. https://doi.org/10.1073/pnas.1516030113.
- Levy, R.H., Meyers, S.R., Naish, T.R., Golledge, N.R., McKay, R.M., Crampton, J.S., Deconto, R.M., De Santis, L., Florindo, F., Gasson, E.G.W., Harwood, D.M., Luyendyk, B.P., Powell, R.D., Clowes, C., Kulhanek, D.K., 2019. Antarctic ice-sheet sensitivity to obliquity forcing enhanced through ocean connections: Sl. Nat. Geosci., 1–14. https://doi.org/10.1038/nature07867.
- Lewis, A.R., Ashworth, A.C., 2015. An early to middle Miocene record of ice-sheet and landscape evolution from the Friis Hills, Antarctica. Geol. Soc. Am. Bull. 128, 719–738. https://doi.org/10.1130/B31319.1.
- Lewis, A.R., Marchant, D.R., Ashworth, A.C., Hedenäs, L., Hemming, S.R., Johnson, J.V., Leng, M.J., Machlus, M.L., Newton, A.E., Raine, J.I., Willenbring, J.K., Williams, M., Wolfe, A.P., 2008. Mid-Miocene cooling and the extinction of tundra in continental Antarctica. Proc. Natl. Acad. Sci. USA 105, 10676–10680. https://doi.org/10.1073/pnas.0802501105.
- Lewis, A.R.R., Marchant, D.R.R., Ashworth, A.C.C., Hemming, S.R.R., Machlus, M.L.L., 2007. Major middle Miocene global climate change: evidence from East Antarctica and the Transantarctic Mountains. Geol. Soc. Am. Bull. 119, 1449. https:// doi.org/10.1130/B26134.
- Meehl, G.A., Senior, C.A., Eyring, V., Flato, G., Lamarque, J.F., Stouffer, R.J., Taylor, K.E., Schlund, M., 2020. Context for interpreting equilibrium climate sensitivity and transient climate response from the CMIP6 Earth system models. Sci. Adv. 6, 1–11. https://doi.org/10.1126/sciadv.aba1981.
- Miller, K.G., Browning, J.V., Schmelz, W.J., Kopp, R.E., Mountain, G.S., Wright, J.D., 2020. Cenozoic sea-level and cryospheric evolution from deep-sea geochemical and continental margin records. Sci. Adv. 6.
- Miller, S.R., Fitzgerald, P.G., Baldwin, S.L., 2010. Cenozoic range-front faulting and development of the Transantarctic Mountains near Cape Surprise, Antarctica: Thermochronologic and geomorphologic constraints. Tectonics 29, 1–21. https:// doi.org/10.1029/2009TC002457.
- Naish, T.R., Powell, R.D., Levy, R., Wilson, G.S., Scherer, R.P., Talarico, F., Krissek, L.A., Niessen, F., Pompilio, M., Wilson, T., Carter, L., DeConto, R.M., Huybers, P., McKay, R.M., Pollard, D., Ross, J., Winter, D., Barrett, P., Browne, G., Cody, R., Cowan, E.A., Crampton, I., Dunbar, G., Dunbar, N., Florindo, F., Gebhardt, C., Graham, I., Hannah, M., Hansaraj, D., Harwood, D.M., Helling, D., Henrys, S., Hinnov, L.A., Kuhn, G., Kyle, P., Läufer, A., Maffioli, P., Magens, D., Mandernack, K., McIntosh, W., Millan, C., Morin, R., Ohneiser, C., Paulsen, T., Persico, D., Raine, I., Reed, I., Riesselman, C.R., Sagnotti, L., Schmitt, D., Siunneskog, C., Strong, P., Taviani, M., Vogel, S., Wilch, T., Williams, T., Barrett, A.P., Browne, G., Cody, R., Cowan, E.A., Crampton, J., Dunbar, G., Dunbar, N., Florindo, F., Gebhardt, C., Graham, I., Hannah, M., Hansaraj, D., Harwood, D.M., Helling, D., Henrys, S., Hinnov, L.A., Kuhn, G., Kyle, P., Läufer, A., Maffioli, P., Magens, D., Mandernack, K., McIntosh, W., Millan, C., Morin, R., Ohneiser, C., Paulsen, T., Persico, D., Raine, I., Reed, J., Riesselman, C.R., Sagnotti, L., Schmitt, D., Sjunneskog, C., Strong, P., Taviani, M., Vogel, S., Wilch, T., Williams, T. Obliquity-paced Pliocene West Antarctic ice sheet oscillations. Nature 458, 322-328. https://doi.org/10.1038/nature07867.
- Ohneiser, C., Wilson, G.S., Beltran, C., Dolan, A.M., Hill, D.J., Prebble, J.G., 2020. Warm fjords and vegetated landscapes in early Pliocene East Antarctica. Earth Planet. Sci. Lett. 534, 116045. https://doi.org/10.1016/j.epsl.2019.116045.
- Passchier, S., Browne, G., Field, B., Fielding, C.R., Krissek, L.A., Panter, K., Pekar, S.F., 2011. Early and middle Miocene Antarctic glacial history from the sedimentary facies distribution in the AND-2A drill hole, Ross Sea, Antarctica. Bull. Geol. Soc. Am. 123, 2352–2365. https://doi.org/10.1130/B30334.1.
- Paxman, G.J.G., Jamieson, S.S.R., Ferraccioli, F., Bentley, M.J., Ross, N., Watts, A.B., Leitchenkov, G., Armadillo, E., Young, D.A., 2019a. The role of lithospheric flexure in the landscape evolution of the Wilkes Subglacial Basin and Transantarctic Mountains, East Antarctica. J. Geophys. Res., Earth Surf. 124, 812–829. https://doi.org/10.1029/2018/F004705.

- Paxman, G.J.G., Jamieson, S.S.R., Hochmuth, K., Gohl, K., Bentley, M.J., Leitchenkov, G., Ferraccioli, F., 2019b. Reconstructions of Antarctic topography since the Eocene– Oligocene boundary. Palaeogeogr. Palaeoclimatol. Palaeoecol. 535, 109346. https://doi.org/10.1016/j.palaeo.2019.109346.
- Pierce, E.L., van de Flierdt, T., Williams, T., Hemming, S.R., Cook, C.P., Passchier, S., 2017. Evidence for a dynamic East Antarctic ice sheet during the mid-Miocene climate transition. Earth Planet. Sci. Lett. 478, 1–13. https://doi.org/10.1016/j. epsl.2017.08.011.
- Pollard, D., DeConto, R.M., 2005. Hysteresis in Cenozoic Antarctic ice-sheet variations. Glob. Planet. Change 45, 9–21. https://doi.org/10.1016/j.gloplacha.2004.09. 011.
- Prentice, M.L., Krusic, A.G., 2005. Early Pliocene Alpine glaciation in Antarctica: terrestrial versus tidewater glaciers in Wright Valley. Geogr. Ann., Ser. A Phys. Geogr. 87, 87–109. https://doi.org/10.1111/j.0435-3676.2005.00246.x.
- Sangiorgi, F., Bijl, P.K., Passchier, S., Salzmann, U., Schouten, S., McKay, R., Cody, R.D., Pross, J., van de Flierdt, T., Bohaty, S.M., Levy, R., Williams, T., Escutia, C., Brinkhuis, H., 2018. Southern Ocean warming and Wilkes Land ice sheet retreat during the mid-Miocene. Nat. Commun. 9, 317. https://doi.org/10.1038/s41467-017-02609-7
- Schnitker, D., 1980. North Atlantic oceanography as possible cause of Antarctic glaciation and eutrophication. Nature 284, 615–616. https://doi.org/10.1038/ 284615a0.
- Shevenell, A.E., Kennett, J.P., Lea, D.W., 2008. Middle Miocene ice sheet dynamics, deep-sea temperatures, and carbon cycling: a Southern Ocean perspective. Geochem. Geophys. Geosyst. 9. https://doi.org/10.1029/2007GC001736.
- Stern, T.A., Baxter, A.K., Barrett, P.J., 2005. Isostatic rebound due to glacial erosion within the Transantarctic Mountains. Geology 33, 221–224. https://doi.org/10.1130/G21068.1.

- Stern, T.A., ten Brink, U.S., 1989. Flexural uplift of the Transantarctic Mountains. J. Geophys. Res., Solid Earth 94, 10315–10330. https://doi.org/10.1029/ JB094iB08p10315.
- Sugden, D.E., Marchant, D.R., Denton, G.H., 1993. The case for a stable East Antarctic ice sheet. Geogr. Ann., Ser. A 75A, 151–351.
- Sugden, D.E., Denton, G.H., Marchant, D.R., 1995. Landscape evolution of the Dry Valleys, Transantarctic Mountains: tectonic implications. J. Geophys. Res. 100, 9949–9967
- Talarico, F.M., Pace, D., Sandroni, S., 2011. Amphibole-bearing metamorphic clasts in ANDRILL AND-2A core: a provenance tool to unravel the Miocene Glacial history in the Ross Embayment, western Ross Sea, Antarctica. Geosphere 7, 922–937. https://doi.org/10.1130/GES00653.1.
- Warny, S., Askin, R.A., Hannah, M.J., Mohr, B.A.R., Raine, J.I., Harwood, D.M., Florindo, F., 2009. Palynomorphs from a sediment core reveal a sudden remarkably warm Antarctica during the middle Miocene. Geology 37, 955–958. https://doi.org/10.1130/G30139A.1.
- Webb, P.N., 1974. Micropaleontology, paleoecology and correlation of the Pecten Gravels, Wright Valley, Antarctica, and description of Trochoelphidiella onyxi n. gen., n. sp. J. Foraminiferal Res. 4, 185–199.
- Wilch, T.I., Denton, G.H., Lux, D.R., McIntosh, W.C., 1993. Limited Pliocene glacier extent and surface uplift in middle Taylor Valley, Antarctica. Geogr. Ann., Ser. A Phys. Geogr. 75, 331–351.
- Willeit, M., Ganopolski, A., Calov, R., Robinson, A., Maslin, M., 2015. The role of CO2 decline for the onset of Northern Hemisphere glaciation. Quat. Sci. Rev. 119, 22–34. https://doi.org/10.1016/j.quascirev.2015.04.015.
- Williams, T., Handwerger, D., 2005. A high-resolution record of early Miocene Antarctic glacial history from ODP Site 1165, Prydz Bay. Paleoceanography 20, 1–17. https://doi.org/10.1029/2004PA001067.